EAST EUROPEAN JOURNAL OF PHYSICS. 3. 336-342 (2025)
DOI:10.26565/2312-4334-2025-3-32 ISSN 2312-4334

ELECTRICAL, OPTICAL, AND STRUCTURAL PROPERTIES OF SILICON n^+-p STRUCTURES

Mykola S. Kukurudziak[a,b]*, Dmytro P. Koziarskyi[a], Ivan P. Koziarskyi[a], Eduard V. Maistruk[a], Maria I. Ilashchuck[a], Dmytro V. Kysil[c]
[a]*Yuriy Fedkovych Chernivtsi National University, Kotsyubyns'kogo str. 2, 58012, Chernivtsi, Ukraine*
[b]*Rhythm Optoelectronics Shareholding Company, Holovna str. 244, 58032, Chernivtsi, Ukraine*
[c]*V.E. Lashkaryov Institute of Semiconductor Physics, NAS of Ukraine, Pr. Nauky 41, 03028, Kyiv, Ukraine*
**Corresponding Author E-mail: mykola.kukurudzyak@gmail.com*
Received April 14, 2025; revised May 7, 2025; accepted August 2, 2025

The article investigates the structural, optical, and electrical properties of silicon n^+-p structures. The experimental samples were made from high-resistance single-crystal silicon using two-stage phosphorus diffusion from solid-state planar sources. It was found that the introduction of phosphorus impurities with a concentration of $1.2 \cdot 10^{20}$ cm^{-3} provokes the formation of dislocations with a surface density of $2 \cdot 10^3$-$3 \cdot 10^3$ cm^{-2} due to the formation and relaxation of mechanical stresses. The formation of a lightening oxide film on the silicon surface reduces the reflection coefficient by 25%. However, the formation of an n^+-layer reduces the transmittance coefficient of the structure. It was established from the voltage-current characteristics of the n^+-p structure under forward and reverse voltage bias, that in the temperature range $T = 295$–346 K, these structures have rectifying properties. At room temperature, the height of the potential barrier is 0.6 eV and decreases with temperature and its height at 0 K is 1.32 eV. At low forward biases, the dominant mechanism of current transport in the structure is superbarrier emission. With an increase in forward voltage from 0.1 V to 0.6 V, the generation-recombination mechanism prevails, and with an increase in temperature, an increase in the contribution of tunnel current is observed. At low reverse voltages, the *I-V* characteristics of diodes are well described by the formula for the generation current. The depth of occurrence of donor energy levels, from which thermal generation of charge carriers occurs is 0.15 eV.
Keywords: *Semiconductors; Thin film; SEM; Electrical conductivity; Structural defects; Reflection; Electromagnetic field sensor; Sensors; Ion implantation; Doping*
PACS: 61.72. Ji, 61.72. Lk, 85.60. Dw

The functioning of virtually all semiconductor devices is based on the physical phenomenon of p-n junction – the boundary between two semiconductor regions with different types of conductivity. Silicon n^+-p junctions are one of the fundamental elements of modern electronics and photonics, due to the high technological capabilities and widespread availability of the base material [1, 2]. Thanks to the combination of a heavily doped n-region (n^+) with p-type silicon, this structure provides unique electrophysical properties that are widely used in power semiconductor devices such as rectifiers [3, 4], thyristors [5, 6], and Schottky diodes [7, 8]. At the same time, n^+-p structures are important for photovoltaic devices, particularly in solar cells [9, 10] electromagnetic field sensors, photodetectors or another sensors [11, 12]. This structure creates an electric field in the depletion region, which allows for effective control of charge carrier movement [13]. Special attention to n^+-p junctions is due to their important role in reducing energy losses, increasing device speed, and improving energy conversion efficiency.

With the growing demand for energy-efficient and compact electronic components, as well as the development of micro- and nanofabrication technologies, n^+-p junctions remain the focus of scientists and developers. Current research focuses on improving doping technologies [14], reducing surface defects [15], passivation [16], and integrating silicon structures with new materials – particularly in the context of creating high-efficiency solar cells and powerful new-generation electronics [17].

Silicon n^+-p junctions can be formed by various methods, including ion implantation and thermal diffusion doping. We have established that the method of doping silicon substrates to create n^+-p junctions and the concentration of the dopant significantly affect the photovoltaic properties of the final products [18]. In particular, phosphorus diffusion from solid-state planar sources [19] allows for low structural defects densities even at high impurity concentrations compared to doping from liquid-phase sources [20]. However, the kinetic and electrical properties of silicon n^+-p structures based on high-resistance base material have not been studied, since most of the work is devoted to low-resistance silicon, which is mainly used for solar cells [9,10, 14, 17]. Thus, the aim of this work is to study the electrical properties of planar n^+-p structures based on high-resistance silicon obtained by phosphorus diffusion from solid sources, and also to investigate the change in the optical and structural properties of silicon after doping.

EXPERIMENTAL

The base material was monocrystalline p-Si with a resistivity of $\rho = 18$-19 kΩ·cm and crystallographic orientation [111]. The experimental samples were silicon substrates with an n^+-p junction formed by two-stage phosphorus diffusion from solid planar sources using the modes given in [18]. The area of the substrates was 28.3 mm^2

Cite as: M.S. Kukurudziak, D.P. Koziarskyi, I.P. Koziarskyi, E.V. Maistruk, M.I. Ilashchuck, D.V. Kysil, East Eur. J. Phys. 3, 336 (2025), https://doi.org/10.26565/2312-4334-2025-3-32

and 500 μm thick. Surface resistance (R_S) was measured using a four-probe method. The surface resistance after phosphorus pre-deposition reached $R_S \approx 4.1$-4.2 Ω/□, and after phosphorus driving-in reached $R_S \approx 2.7$-2.8 Ω/□. The antireflective SiO_2 on the surface of the experimental samples was formed by oxidation in a dry oxygen atmosphere during phosphorus driving-in and reached $d_{SiO2} = 180$-200 nm.

The depth of the diffusion layer (x_{n+-p}) was measured using scanning electron microscopy (SEM, Tescan Lyra 3). To investigate the defective structure of the silicon substrates chemical treatment was performed in selective Sirtle`s etchant [20] with the following composition: HF—100 cm^3, CrO_3 50 g, H_2O—120 cm^3. The density of dislocations was calculated by the metallographic method [21]. The transmission spectra were investigated using NIKOLET 6700 and SF-2000 spectrophotometer at room temperature. For measuring reflection (R) UV-Vis spectrophotometer Specord 210 plus was used. Reflection spectra were measured in total reflection geometry using additional equipment – an integrating sphere. The I-V characteristics (at $T = 295$-346 K) of the samples were measured using a hardware-software complex implemented on the basis of the Arduino platform, an Agilent 34410 A digital multimeter and a Siglent SPD3303X programmable power source, which were controlled by a personal computer using software created by the authors in the LabView environment. Experimental studies of kinetic phenomena in silicon n^+-layers were conducted in the temperature range $T = 290$-380 K based on measurements of the Hall effect in film structures [22], considers that the n^+-layer is a thin film.

RESULTS OF THE RESEARCH AND THEIR DISCUSSION

A) Structural and optical properties of silicon n^+-p structures

After phosphorus pre-deposition, the depth of the diffusion layer reached $x_{n+-p} = 0.8$–1 μm, and after driving-in, it reached $x_{n+-p} = 4.2$–4.4 μm (Fig. 1). The measurements correlate well with the values obtained by the layer-slab method.

The density of dislocations in the base silicon reached about $N_{dis} = 10$-20 cm^{-2} (Fig. 2a). After phosphorus diffusion, the density of structural defects increased to $N_{dis} = 2 \cdot 10^3$-$3 \cdot 10^3$ cm^{-2} (Fig. 2b). The increase in the density of structural defects is caused by the introduction of an impurity with a larger atomic radius than silicon, which leads to the emergence of mechanical stresses. Accordingly, their relaxation during heat treatment occurs with the formation of dislocations [23]. However, such an increase in defect density does not lead to a significant deterioration in the electrophysical characteristics of structures [24].

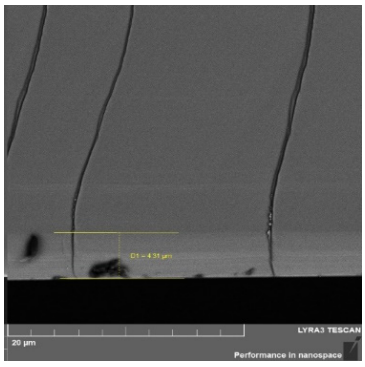

Figure 1. SEM photo of a silicon substrate chip with an n^+-layer

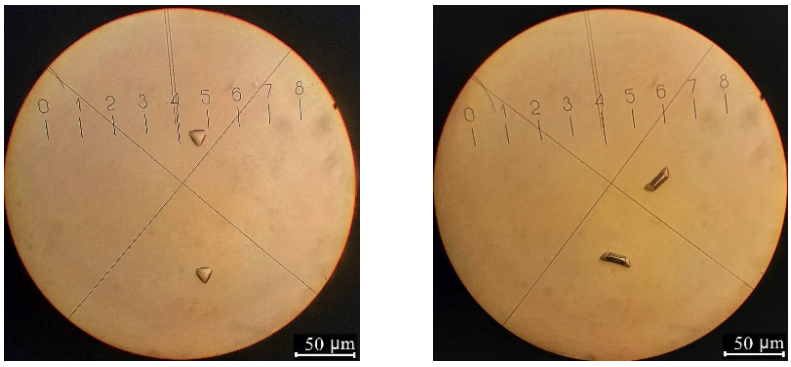

a b

Figure 2. Images of dislocations on the surface of p-Si (a) and n^+-Si (b)

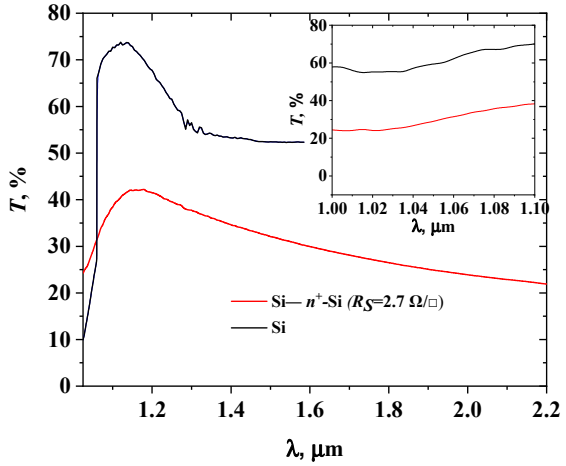

Figure 3. The transmission spectrum of silicon and its n^+-p structure (without SiO_2) (inset the range of λ = 1-1.1 μm)

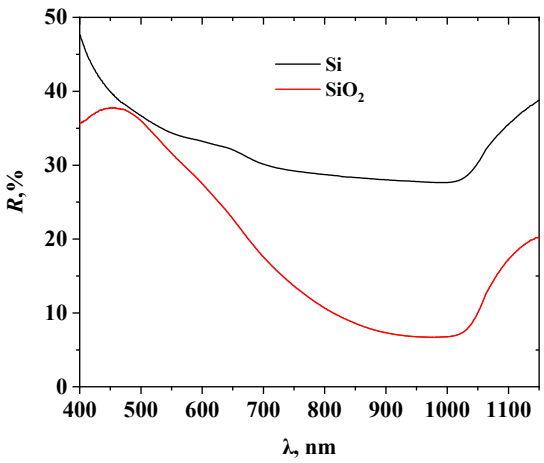

Figure 4. Reflection spectrum of Si and SiO_2

The formation of n^+-layers on the Si surface causes a significant decrease in the transmission coefficient of structures (Fig. 3), which is negative in the case of the need to ensure radiation absorption in the high-resistance region of the structure, for example, in the manufacture of *p-i-n* photodiodes [25]. Thus, in the range of λ = 1-1.1 μm (Fig. 3 inset), the difference in the transmittance coefficients of Si and silicon n^+-*p* structure reaches about 30%. This difference increases with increasing wavelengths.

However, the formation of SiO_2 on the surface of n^+-*p* structure significantly reduces the coefficient of radiation reflection compared to the case without thin film of oxide (Fig. 4). Thus, in the case under study, the difference in reflection coefficients in the range of 950-1050 nm reached about 25%, since the obtained thickness of SiO_2 corresponds to the condition of minimum reflection for these wavelengths [26].

B) Kinetic properties of silicon n^+-layers

Studies of silicon n^+-layers at T = 290-380 K showed that the Hall coefficient in this temperature range remains practically unchanged (Fig. 5). This indicates that at these temperatures, the concentration of charge carriers does not change (Fig. 5 inset), due to the depletion of impurity levels at these temperatures [22]. The electron concentration reached about $n \approx 1.2 \cdot 10^{20}$ cm^{-3}, which correlates well with the phosphorus concentrations determined in [19].

With increasing temperature, a decrease in electrical conductivity is observed (Fig. 6) due to a decrease in Hall mobility (Fig. 6 inset), since in this temperature range, charge carriers are scattered by thermal vibrations of the crystal lattice.

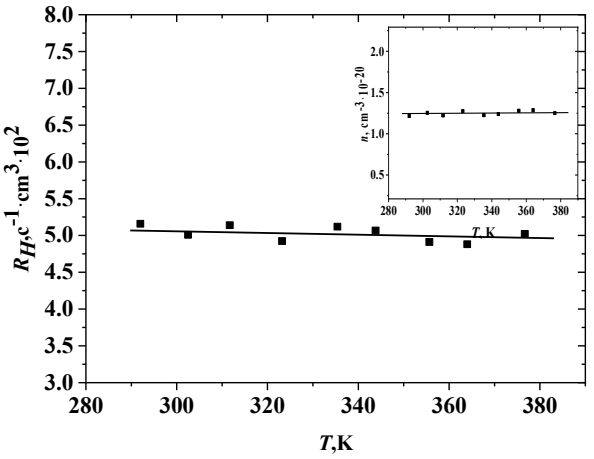

Figure 5. Temperature dependence of the Hall coefficient and electron concentration (inset) in a silicon n^+-layer

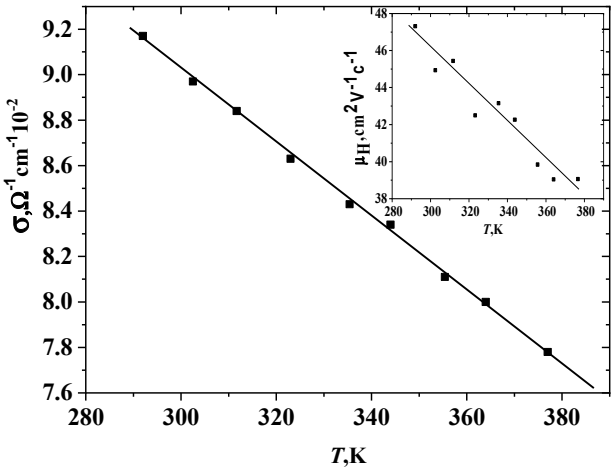

Figure 6. Temperature dependence of electrical conductivity and Hall mobility (inset) of a silicon n^+-layer

C) Electrical properties of silicon n^+-layers

From the voltage-current characteristics of the n^+-*p* structure at forward (Fig. 7) and reverse (Fig. 8) bias voltages, it can be seen that in the temperature range T = 295 – 346 K, these structures have rectifying properties. The rectification coefficient determined at T = 295 K and voltages $|V|$ = 0.6 V is equal to $RR \sim 10^5$.

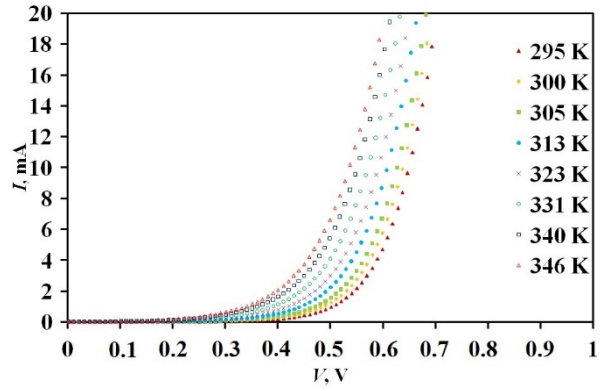

Figure 7. *I-V* characteristics of the n^+-*p* junction at forward biases in the temperature range from 297 K to 346 K

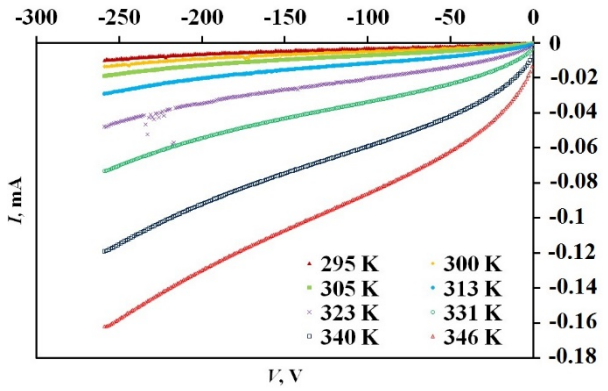

Figure 8. *I-V* characteristics of the n^+-*p* junction at reverse biases in the temperature range from 297 K to 346 K

The height of the potential barrier ($q\varphi_k$) was estimated by extrapolating the linear sections of the *I-V* characteristics in the forward voltage bias region. At room temperature, the height of the potential barrier is $q\varphi_k \sim 0.6$ eV and decreases with temperature (Fig. 9).

When the temperature is increased from $T = 295$ K to $T = 346$ K (Fig. 9), there is a linear decrease in the energy $q\varphi_k$ from 0.6 eV to 0.49 eV. This dynamic change occurs as a result of a decrease in the height of the potential barrier and is described by the equation [27]:

$$q\varphi_k(T) = q\varphi_k(0) - \beta_\varphi T \quad (1)$$

where β_φ is the temperature coefficient of the potential barrier height, and $q\varphi_k(0)$ is the value of the potential barrier height of the n^+-p structure at absolute zero temperature.

Using equation (1) and Fig. 9, we find the temperature coefficient of change in the height of the potential barrier and its height at 0 K, which are equal to $d(q\varphi_k)/dT = -2.45 \cdot 10^{-3}$ eV/K i $q\varphi_k(0\ \text{K}) = 1.32$ eV, respectively.

Based on the values of the sequential resistance R_S of the structure determined at different temperatures along the linear sections of the direct branches of the I-V curve, the temperature dependence $lnR_S = f(10^3/T)$ was constructed (Fig. 10) and the activation energy $E_A = 0.25$ eV was determined, which characterizes the temperature dependence of the electrical conductivity of the structure components.

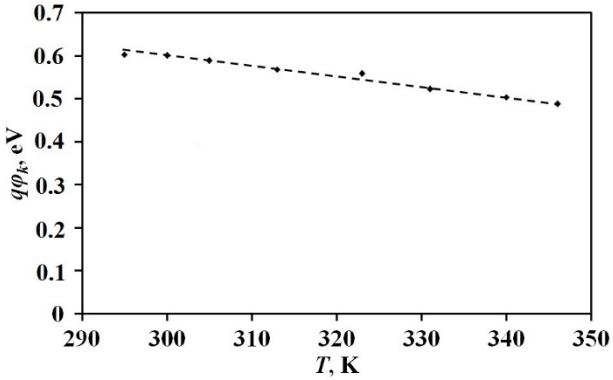

Figure 9. Temperature dependence of the height of the potential barrier

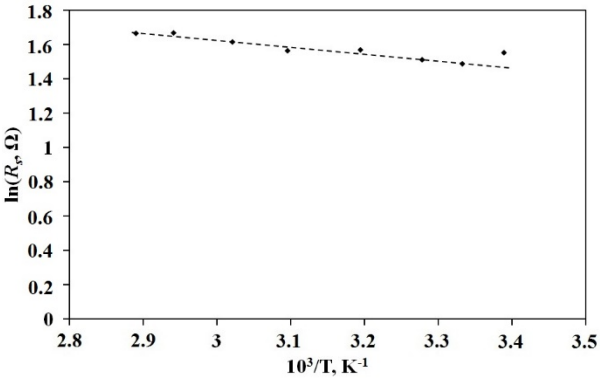

Figure 10. Temperature dependence of series resistance

To determine the mechanism of current flow through the junction at forward bias, the I-V characteristics are plotted in the coordinates $lnI = f(V)$ (Fig. 11). Fig. 11 shows two straight segments with different angles of inclination to the voltage axis. Based on the tangents of these angles, we determine the coefficient of n^+-p junction imperfection n (Fig. 12).

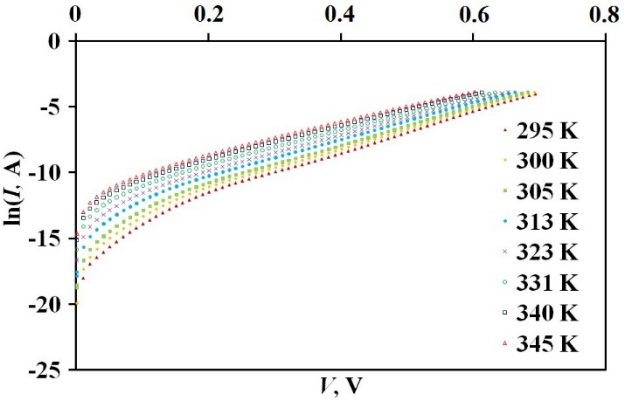

Figure 11. Temperature dependencies of $lnI = f(V)$ n^+-p junction at forward bias

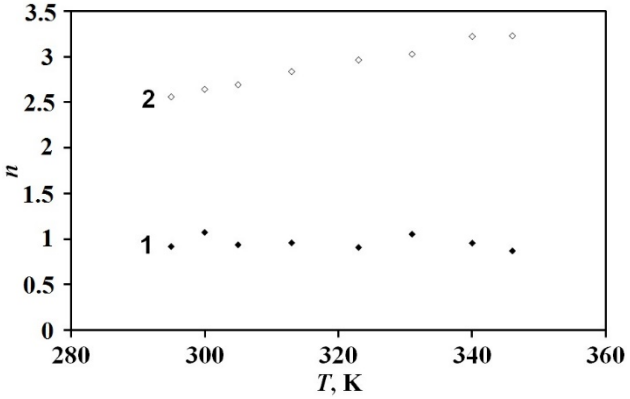

Figure 12. Temperature dependence of the imperfection coefficient at forward bias:
1 - $3kT/q < V < 0.1$ V; 2 – 0.1 V < V < 0.6 V

At small forward biases $3kT/q < V < 0.1$ V, the slope to the voltage axis of linear dependencies $lnI = f(V)$ is characterized by the value of the imperfection coefficient $n \approx 1$ (Fig. 12-1), accordingly, the dominant mechanism of current transport is superbarrier emission. With an increase in direct voltage 0,1 V < V < 0.6 V, the imperfection coefficient is equal to $n \approx 2.5$ - 3 (Fig. 12-2), which indicates the predominance of the generation-recombination mechanism of current transport at room temperatures and an increase in the contribution of the tunnel current with increasing temperature.

It can be assumed that, in some approximation, the I-V characteristics of diodes are described by the equation for the recombination current density [23]:

$$j = \frac{qn_iW_i}{\tau}\left(e^{\frac{qV}{2kT}} - 1\right) = \frac{n_i}{\tau}\sqrt{\frac{2q}{N_A}(\phi_k - V)}\left(e^{\frac{qV}{2kT}} - 1\right), \quad (2)$$

where q is the charge of electron, n_i is the value of the intrinsic concentration of charge carriers, W_i is the thickness of the depleted region, τ is the lifetime of charge carriers in this region, and N_A is the concentration of acceptor impurities.

At low reverse voltages, the *I-V* characteristics of struscures are well described by the formula for the generation current (the multiplier before the brackets in expression 2), which is confirmed by the linear nature of the dependencies $I = f(\varphi_k - V)^{1/2}$ (Fig. 13).

Determined from the dependence $lnI_{rev} = f(10^3/T)$ (Fig. 14), obtained at a constant voltage value, the depth of the acceptor energy levels from which thermal generation of charge carriers occurs was $\Delta E \approx 0.15$ eV at -100 < V < 0 V.

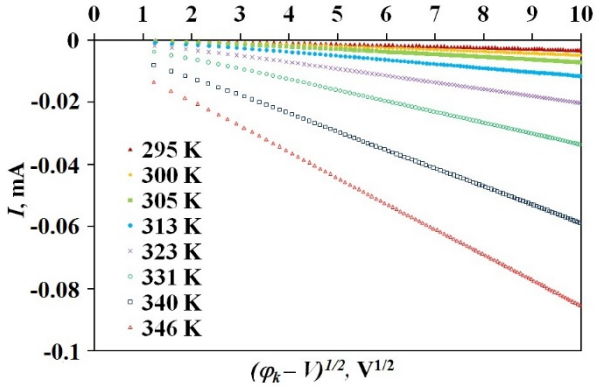

Figure 13. Reverse branches of *I-V* characteristics in coordinates $I = f(\varphi_k - V)^{1/2}$ at different temperatures

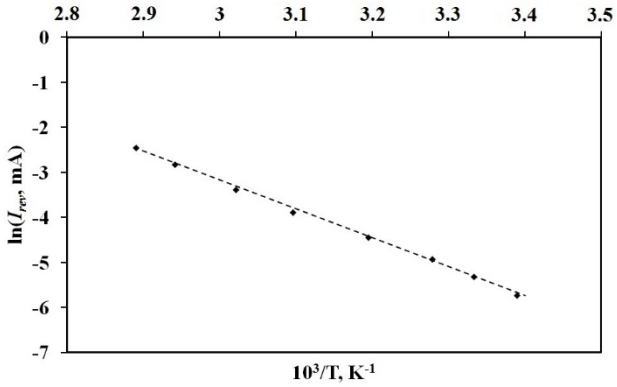

Figure 14. Dependence of $lnI_{rev} = f(10^3/T)$ at reverse bias

The reverse branches of the *I-V* characteristic at temperatures T = 295–346 K are described by the equation for tunnel current [27]:

$$I_t = a_0 \, exp\left(-b_0(\phi_k - V)^{-1/2}\right), \tag{3}$$

where a_0 is a parameter, whose value is determined by the probability of filling the energy levels from which electron tunneling occurs, b_0 is determined by the rate of change of the current with voltage.

According to (2), the reverse *I-V* curves in the coordinates $ln(I_{rev}) = f(\varphi_k - qV)^{-1/2}$ will be linear, as observed in Fig. 15.

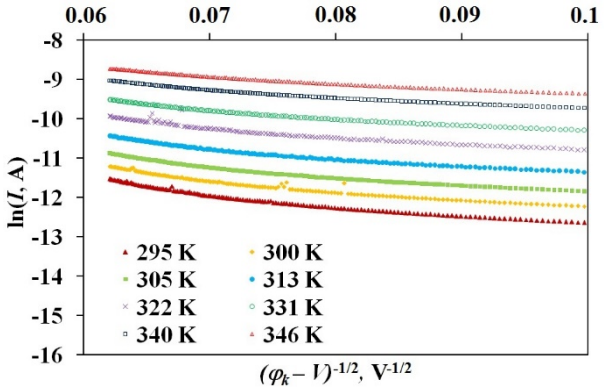

Figure 15. Dependence of tunnel current on reverse external displacement in the temperature range T = 295-346 K

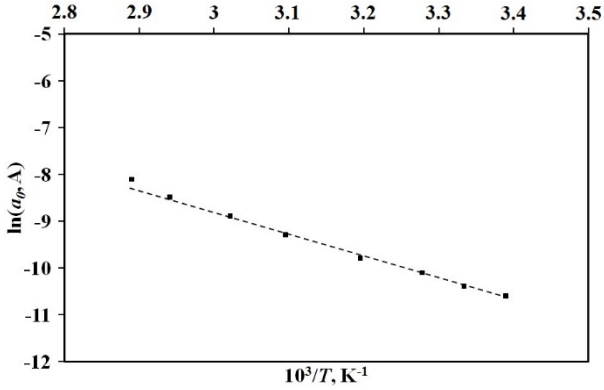

Figure 16. Dependence $lga_0 = f(10^3/T)$ at reverse bias

The energy level value at large reverse biases (-100 < V), from which electron tunneling occurs, was calculated from the temperature dependence of the parameter a_0, which in the coordinates $lga_0 = f(10^3/T)$ is approximated by a straight line (Fig. 16). The parameter a_0 was determined by extrapolating the straight sections $ln(I_{rev}) = f(\varphi_k - qU_{зм})^{-1/2}$ to the current axis. The established depth of the energy level was 0.2 eV.

CONCLUSIONS

The structural, optical, and electrical properties of n^+-p structures of high-resistance silicon were investigated. The following conclusions were made during the research:

1. The introduction of phosphorus impurities with a concentration of $1.2 \cdot 10^{20}$ cm^{-3} provokes the formation of dislocations with a surface density of $2 \cdot 10^3$-$3 \cdot 10^3$ cm^{-2}

2. The formation of anti-reflective SiO_2 on the silicon surface reduces the reflection coefficient by 25%.

3. The formation of an n^+-layer reduces the transmittance coefficient of the structure relative to the transmittance coefficient of silicon.

4. At room temperature, the height of the potential barrier of the n^+-p structure is 0.6 eV and decreases with increasing temperature, and its height at 0 K is 1.32 eV.

5. At low forward voltages, the dominant mechanism of current flow in the structure is superbarrier emission. With an increase in forward voltage, the generation-recombination mechanism prevails, and with an increase in temperature, an increase in the contribution of tunnel current is observed.

6. At low reverse voltages, the generation mechanism of current transport prevails.

Acknowledgments

This work was partially supported by the Ministry of Education and Science of Ukraine (grant number 0125U000832, Rational design of quaternary detector materials for remote devices operating in conditions of significant radiation exposure, authors M.S. Kukurudziak).

ORCID

Mykola S. Kukurudziak, https://orcid.org/0000-0002-0059-1387; **Dmytro P. Koziarskyi,** https://orcid.org/0000-0002-9618-0418;
Ivan P. Koziarskyi, https://orcid.org/0000-0002-4984-4349; **Eduard V. Maistruk**, https://orcid.org/0000-0002-9025-6485;
Maria I. Ilashchuck, https://orcid.org/0000-0002-7618-0437; **Dmytro V. Kysil,** https://orcid.org/0000-0003-4637-9397

REFERENCES

[1] C. Ballif, F.J. Haug, M. Boccard, P.J. Verlinden, and G. Hahn, Nature Reviews Materials, **7**(8), 597 (2022). https://doi.org/10.1038/s41578-022-00423-2
[2] X. Pan, S. Li, Y. Li, P. Guo, X. Zhao, and Y. Cai, Minerals Engineering, **183**, 107600 (2022). https://doi.org/10.1016/j.mineng.2022.107600
[3] B.J. Baliga, IEEE Journal of Emerging and Selected Topics in Power Electronics, **11**(3), 2400-2411 (2023). https://doi.org/10.1109/JESTPE.2023.3258344
[4] R. Gupta, J.A. Fereiro, A. Bayat, A. Pritam, M. Zharnikov, and P.C. Mondal, Nature Reviews Chemistry, **7**(2), 106-122 (2023). https://doi.org/10.1038/s41570-022-00457-8
[5] C. Shen, S. Jahdi, O. Alatise, J. Ortiz-Gonzalez, A. Aithal, and P. Mellor, IEEE Open Journal of Power Electronics, **2**, 145-154 (2021). https://doi.org/10.1109/OJPEL.2021.3060942
[6] M. Faizan, X. Wang, and M. Z. Yousaf. Electronics, **12**(13), 2850 (2023). https://doi.org/10.3390/electronics12132850
[7] J.O. Bodunrin, D.A. Oeba, and S.J. Moloi, Sensors and Actuators A: Physical, **331**, 112957 (2021). https://doi.org/10.1016/j.sna.2021.112957
[8] Z. Berktaş, M. Yıldız, E. Seven, E.O. Orhan, and Ş. Altındal. Flat. Chem. **36**, 100436 (2022). https://doi.org/10.1016/j.flatc.2022.100436
[9] H. Zhang, X. Wang, X. Chen, and Y. Zhang, Nano Energy, 110715 (2025). https://doi.org/10.1016/j.nanoen.2025.110715
[10] M.A., Green, and Z. Zhou, Nature Communications, **16**(1), 251(2025). https://doi.org/10.1038/s41467-024-55681-1
[11] R.L. Politanskyi, P.M. Shpatar, M.V. Vistak, I.T. Kogut, I.S. Diskovskyi, and Y.A. Rudyak, Physics and Chemistry of Solid State, **24**(3), 433-440 (2023). https://doi.org/10.15330/pcss.24.3.433-440
[12] M.S. Kukurudziak, and E.V. Maistruk, in: *Fifteenth International Conference on Correlation Optics*, 121261V (SPIE, Chernivtsi, 2021). https://doi.org/10.1117/12.2616170
[13] I.P. Koziarskyi, E.V. Maistruk, I.G. Orletskyi, M.I. Ilashchuk, D.P. Koziarskyi, P.D. Maryanchuk, M.M. Solovan, and K.S. Ulyanytskiy, Semiconductor Science and Technology, **35**(2), 025018 (2020). https://doi.org/10.1088/1361-6641/ab6107
[14] I. García, in: *Fundamentals of Solar Cells and Photovoltaic Systems Engineering*, (Academic Press, 2025), pp. 129-171. https://doi.org/10.1016/B978-0-323-96105-9.00005-7
[15] F.L. Via, M. Zimbone, C. Bongiorno, A. La Magna, G. Fisicaro, I. Deretzis, and P. Wellmann, Materials, **14**(18), 5348 (2021). https://doi.org/10.3390/ma14185348
[16] J. Panigrahi, and V.K. Komarala, Journal of non-crystalline solids, **574**, 121166 (2021). https://doi.org/10.1016/j.jnoncrysol.2021.121166
[17] J. Pastuszak, and P. Węgierek, "Photovoltaic cell generations and current research directions for their development," Materials, **15**(16), 5542 (2022). https://doi.org/10.3390/ma15165542
[18] M.S. Kukurudziak, Semiconductor Physics, Quantum Electronics & Optoelectronics, **25**(4), 385 (2022). https://doi.org/10.15407/spqeo25.04.385
[19] M.S. Kukurudziak, Physics and Chemistry of Solid State, **23**(4), 756 (2022). https://doi.org/10.15330/pcss.23.4.756-763
[20] E. Sirtl, and A. Adler, International Journal of Materials Research, **52**(8), 529 (1961). https://doi.org/10.1515/ijmr-1961-520806 (in German)
[21] S.N. Knyazev, A.V. Kudrya, N.Y. Komarovsky, Y.N. Parkhomenko, E.V. Molodtsova, and V.V. Yushchuk, Electron. Eng. Mater. **25**, 323–36 (2023). https://doi.org/10.3897/j.moem.8.4.99385
[22] E.V. Maystruk, T.T. Kovalyuk, M.M. Solovan, and P.D. Maryanchuk. Journal of Nano- and Electronic Physics, **10**(5), 05028 (2018). https://10.21272/jnep.10(5).05028
[23] K.V. Ravi, *Imperfections and impurities in semiconductor silicon*, (Wiley, New York, 1981).
[24] M.S. Kukurudziak, East Eur. J. Phys. (2), 345 (2024). https://doi.org/10.26565/2312-4334-2024-0-41
[25] M.S. Kukurudziak, E.V. Maistruk, East Eur. J. Phys. (1), 386 (2024), https://doi.org/10.26565/2312-4334-2024-1-39
[26] S.B. Khan, S. Irfan, Z. Zhuanghao, and S.L. Lee, Materials, **12**(9), 1483 (2019). https://doi.org/10.3390/ma12091483
[27] H.P. Parkhomenko, M.M. Solovan, A.I. Mostovyi, I.G. Orletskyi, and V.V. Brus, East. Eur. J. Phys. (4), 43 (2021). https://doi.org/10.26565/2312-4334-2021-4-04

ЕЛЕКТРИЧНІ, ОПТИЧНІ ТА СТРУКТУРНІ ВЛАСТИВОСТІ КРЕМНІЄВИХ n^+-p СТРУКТУР

Микола С. Кукурудзяк[a,b], Дмитро П. Козярський[a], Іван П. Козярський[a], Едуард В. Майструк[a], Марія І. Ілащук[a], Дмитро В. Кисіль[c]

[a]*Чернівецький національний університет імені Юрія Федьковича, 58002, м. Чернівці, вул. Коцюбинського, 2, Україна*

[b]*АТ «Центральне конструкторське бюро Ритм», 58032, м. Чернівці, вул. Головна, 244, Україна*

[c]*Інститут фізики напівпровідників ім. В.Е. Лашкарьова, НАН України, 03028, м. Київ, пр. Науки, 41, Україна*

У статті досліджено структурні, оптичні та електричні властивості кремнієвих n^+-p структур. Експериментальні зразки були виготовлені з високоомного монокристалічного кремнію з використанням двостадійної дифузії фосфору з твердотільних планарних джерел. Було встановлено, що введення домішок фосфору з концентрацією $1{,}2\cdot10^{20}$ см$^{-3}$ провокує утворення дислокацій з поверхневою густиною $2\cdot10^3$-$3\cdot10^3$ см$^{-2}$ внаслідок утворення та релаксації механічних напружень. Утворення противідбиваючої оксидної плівки на поверхні кремнію зменшує коефіцієнт відбиття на 25 %. Однак утворення n^+-шару зменшує коефіцієнт пропускання структури. З вольт-амперних характеристик n^+-p структур при прямому та зворотному зміщенні напруги було встановлено, що в діапазоні температур T = 295–346 K ці структури мають випрямні властивості. При кімнатній температурі висота потенційного бар'єру становить 0,6 еВ і зменшується з підвищенням температури, а його висота при 0 K становить 1,32 еВ. При низьких прямих напругах домінуючим механізмом струмопереносу в структурі є надбар'єрна емісія. Зі збільшенням прямої напруги від 0,1 В до 0,6 В переважає механізм генерації-рекомбінації, а зі збільшенням температури спостерігається збільшення внеску тунельного струму. При низьких зворотних напругах вольт-амперні характеристики діодів добре описуються формулою для струму генерації. Глибина залягання енергетичного донорного рівня, з якого відбувається теплова генерація носіїв заряду, становить 0,15 еВ.

Ключові слова: *напівпровідники; тонкі плівки; SEM; електропровідність; структурні дефекти; відбиття; датчик електромагнітного поля; датчики; іонна імплантація; легування*